

Article

Synthesis of Hydroxylammonium Nitrate and Its Decomposition over Metal Oxide/Honeycomb Catalysts

Dalsan Yoo ¹, Munjeong Kim ¹, Seung Kyo Oh ¹, Seoyeon Hwang ¹, Sohee Kim ², Wooram Kim ², Yoonja Kwon ², Youngmin Jo ²  and Jong-Ki Jeon ^{1,*}

¹ Department of Chemical Engineering, Kongju National University, Cheonan 31080, Republic of Korea; qv2846@smail.kongju.ac.kr (D.Y.); veronica9605@smail.kongju.ac.kr (M.K.); seungkyo@smail.kongju.ac.kr (S.K.O.); tjds4788@gmail.com (S.H.)

² Department of Environmental Science and Engineering, Kyung Hee University, Yongin 17104, Republic of Korea; 2019310448@khu.ac.kr (S.K.); woojoa@hanmail.net (W.K.); silvia@khu.ac.kr (Y.K.); ymjo@khu.ac.kr (Y.J.)

* Correspondence: jkjeon@kongju.ac.kr

Abstract: The objectives of this study were to prepare a high-purity hydroxylammonium nitrate (HAN) solution and evaluate the performance of various types of metal oxide/honeycomb catalysts during the catalytic decomposition of the HAN solution. Hydroxylammonium nitrate was prepared via a neutralization reaction of hydroxylamine and nitric acid. FT-IR was used to analyze the chemical composition, chemical structure, and functional groups of the HAN. The aqueous HAN solution obtained from pH 7.06 showed the highest concentration of HAN of 60% and a density of 1.39 g/mL. The concentration of HAN solution that could be obtained when the solvent was evaporated to the maximum level could not exceed 80%. In this study, catalysts were prepared using a honeycomb structure made of cordierite (5SiO₂-2MgO-2Al₂O₃) as a support, with Mn, Co, Cu, Pt, or Ir impregnated as active metals. The pore structure of the metal oxide/honeycomb catalysts did not significantly depend on the type of metal loaded. The Cu/honeycomb catalyst showed the strongest effect of lowering the decomposition onset temperature in the decomposition of the HAN solution likely due to the intrinsic activity of the Cu metal being superior to that of the other metals. It was confirmed that the effect of the catalyst on the decomposition mechanism of the aqueous HAN solution was negligible. Through a repetitive cycle of HAN decomposition, it was confirmed that the Cu/honeycomb catalyst could be recovered and reused as a catalyst for the decomposition of an aqueous HAN solution.

Keywords: hydroxylammonium nitrate; synthesis; liquid monopropellant; catalytic decomposition; honeycomb catalyst



Citation: Yoo, D.; Kim, M.; Oh, S.K.; Hwang, S.; Kim, S.; Kim, W.; Kwon, Y.; Jo, Y.; Jeon, J.-K. Synthesis of Hydroxylammonium Nitrate and Its Decomposition over Metal Oxide/Honeycomb Catalysts. *Catalysts* **2024**, *14*, 116. <https://doi.org/10.3390/catal14020116>

Academic Editors: Chaoqiu Chen, Xin Jin, Xiao Chen, Jinshu Tian and Lihua Zhu

Received: 30 December 2023

Revised: 26 January 2024

Accepted: 29 January 2024

Published: 31 January 2024



Copyright: © 2024 by the authors. Licensee MDPI, Basel, Switzerland. This article is an open access article distributed under the terms and conditions of the Creative Commons Attribution (CC BY) license (<https://creativecommons.org/licenses/by/4.0/>).

1. Introduction

At present, artificial satellite technology does not allow additional fuel to be supplied in the universe, and thus, fuel is the most important variable during the service lifetime of an artificial satellite. The performance and efficiency of fuel for an artificial satellite can be maximized by utilizing a catalyst in the thruster, which can secure stable posture control and extend the operation period of the artificial satellite [1,2]. A common liquid monopropellant for artificial satellites is hydrazine (N₂H₄). In order to secure driving force through the effective decomposition of hydrazine monopropellants within a thruster, various types of catalysts have been used, including Shell 405, which impregnates iridium metals on γ -Al₂O₃ [2–4].

Given that hydrazine monopropellants enable decomposition even at a low temperature by means of a catalyst, being able to decrease the ignition temperature drastically is one of the advantages [5,6]. On the other hand, hydrazine is highly toxic to human respiratory organs and skin. Moreover, hydrazine decomposition generates halogen compounds,

which is a serious threat to human health. Proper handling and storage of this material can be both expensive and risky [2–4,7–11]. Since 2011, when hydrazine and its derivatives were added to the list of substances of very high concern (SVHC), research on eco-friendly, low-toxicity liquid propellants has drawn keen attention [1,5,9,12].

Eco-friendly, low-toxicity liquid propellants that have been topics of research as alternatives to hydrazine include hydrogen peroxide, ammonium dinitramide (ADN), and hydroxyl ammonium nitrate (HAN) [2,8–10,12–17]. Among these, HAN features superior specific thrust to hydrazine, a high level of density, a low freezing point, and outstanding stability. Hence, HAN is advantageous in terms of fuel efficiency, fuel performance, handling, and storage. In addition, it is very eco-friendly, being less toxic than LMP-103S, which is an ADN-based monopropellant [7,9,18]. HAN is an ionized liquid oxidizer that consists of nitrogen, which is a fuel element, and oxygen and hydrogen, which are oxidizing agents. It may remain dissociated in an ion form such as NH_3OH^+ and NO_3^- or combined in the form of NH_3OHNO_3 in a solution [19].

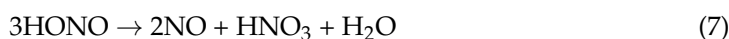
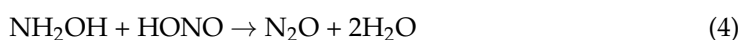
The HAN compound synthesis process includes the following methods: a method to cause the reaction of hydroxyl ammonium sulfate [HAS, $(\text{NH}_2\text{OH})_2\cdot\text{H}_2\text{SO}_4$] and barium nitrate (BaNO_3) [20], a method that causes HAS and ammonia in ethanol to undertake ion exchange with nitric acid [21], a method that causes the reaction of HAS and sodium nitrate (NaNO_3) in n-butyl alcohol ($\text{C}_4\text{H}_9\text{OH}$) [22], and so forth. In general, a method that causes HAS to react to a saturated barium nitrate solution and a concentration for HAN poses some problems: The initial stage results in barium chloride, lowering the purity of the final HAN, and the by-products of barium sulfate resulting from the synthesis process must be removed.

In order to overcome such challenges, this study aims to develop a method that minimizes the formation of intermediates with liquid hydroxylamine (HA, NH_2OH) as the starting material. Specifically, aqueous-phase hydroxylamine was selected as the starting material, as shown in Equation (1), and nitric acid was added for neutralization in order to induce an acid–base reaction [23,24].



Weak-base hydroxylamine was selected as the starting material instead of nitric acid, which is a strong acid that was used in order to reduce the heat-generating reaction in the neutralization process. In addition, in the event that a reaction begins in the reactor with nitric acid as the starting material, it is probable that the nitric acid would cause fumes prior to the proper addition of hydroxylamine, thus decreasing the efficiency of HAN generation. In this study, therefore, hydroxylamine was used as the starting material to form HAN at a consistent density.

In order to apply HAN as an ionic liquid propellant, a high level of stability is required. For this purpose, it must be dissolved in H_2O [3,25]. Previously, it was reported that there are eight decomposition pathways, expressed here as Equations (2)–(9) for the aqueous HAN solution, as follows [26]:



HAN-based liquid propellants are disadvantageous in terms of ignition due to the high moisture content. Since decomposition is essential for ignition of a HAN aqueous solution, heating is necessary to induce a decomposition reaction, and thus, preheating is required. Since energy consumption needs to be minimized due to the spatial limitation inside an artificial satellite, it is necessary to keep the decomposition temperature as low as possible by means of a catalyst. Once a liquid propellant starts decomposition in the artificial satellite thruster, ignition is initiated and the catalyst bed temperature increases intermittently to as high as 1200 °C. Since contact decomposition used in posture control of an artificial satellite is repeated, a catalyst with high heat resistance is essential. Specifically, a catalyst for the decomposition of liquid propellants in the artificial satellite thruster needs to activate decomposition at a low temperature, and at the same time, requirements for high heat resistance and high mechanical intensity need to be met as well [8,11,27].

Various types of catalysts such as beads, pellets, granules, or honeycombs can be used for the satellite thruster. Honeycomb catalysts offer superior advantages, including high surface areas, low pressure drops, uniform flow distributions, enhanced heat transfer characteristics, good mechanical stability, controlled thicknesses, a compact design, and ease of integration, making them efficient and versatile compared to bead, pellet, or granule catalysts in various chemical processes. With the honeycomb catalyst, a chemical reaction occurs as a reactant passes through a cell on which the catalyst is supported. Therefore, one advantage of a honeycomb catalyst is that the pressure drop is minor because the diffusion of reactants and products is less limited [28]. Meanwhile, honeycomb made from cordierite (MgO-SiO₂-Al₂O₃) is used as a highly heat-resistant support [29,30]. It has been reported that iridium is useful as an active ingredient in catalysts for the decomposition of energetic ionic liquids [31]. However, iridium is expensive, and thus, it is necessary to evaluate the activity and stability of other metals that can be an alternative.

In this study, catalysts were prepared using honeycomb made of cordierite (5SiO₂-2MgO-2Al₂O₃) as a support, and Mn, Co, Cu, Pt, or Ir was impregnated as an active metal. The physicochemical properties of the catalyst samples were investigated using X-ray diffraction (XRD), nitrogen adsorption, X-ray fluorescence (XRF), and scanning electron microscopy (SEM). The catalytic performance during the decomposition of aqueous HAN solution was evaluated using a batch reactor. In addition, the decomposition activity of the aqueous HAN solution was evaluated repeatedly, and the effects of catalyst composition and morphology on decomposition activity, durability, and heat resistance were investigated.

To clarify the objectives of this study, the primary objective is to propose a method with which to prepare HAN solutions using liquid hydroxylamine and nitric acid as starting materials. Secondary objectives are to evaluate the performance capabilities of different types of metal oxide/honeycomb catalysts with regard to the catalytic decomposition of HAN solutions and to verify the reusability using the best catalyst.

2. Results and Discussion

2.1. Synthesis of Hydroxylammonium Nitrate

Figure 1 shows the effects of the hydroxylamine/nitric acid ratio on the pH and content of HAN in the HAN synthesis process as high-density nitric acid was added to hydroxylamine. In the initial stage, the pH of hydroxylamine was 9 and that of the nitric acid used in the synthesis was 1. Hence, as the quantity of nitric acid increased, the quantity of nitrogen ions in the nitric acid increased, whereas the pH of the HAN in the aqueous phase decreased. In general, synthesized HAN can generate hydroxylamine and nitric acid in a reversible reaction that proceeds according to Equation (10).



With regard to the mechanism of this reaction, it is known that as the number of nitric acid ions is reduced, the amount of nitrous acid (HNO₂) or nitroxyl (HNO) increases [12]. It is also known that HAN decomposition continues according to Equation (3). It is necessary,

therefore, to secure environments where the HAN manufacturing yield is maximized in such reversible reactions.

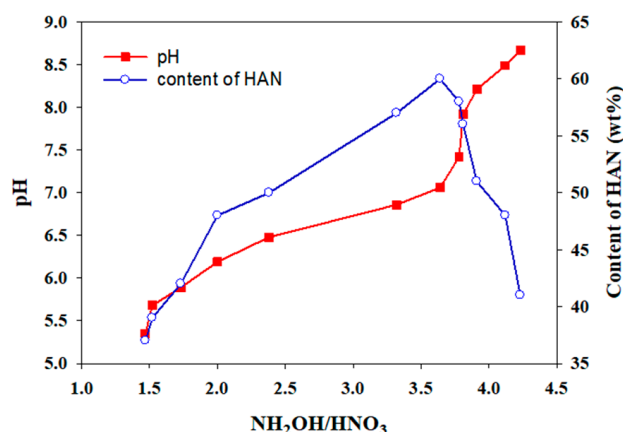


Figure 1. Effects of the hydroxylamine/nitric acid ratio on the pH and content of HAN.

When HAN-based energetic compounds in an aqueous solution are utilized as a mono-propellant, the energy quantity and heat generation characteristics are determined based on the actual HAN content. However, it is difficult to directly measure the concentration of HAN in an ionized form. Hence, the empirical model to estimate the concentration indirectly by measuring the density of an aqueous solution (Equation (11)) is commonly utilized [32].

$$\rho = \frac{107.85}{96.042 - w(\text{HAN}) \times 30.99} \quad (11)$$

Figure 1 shows the concentration of HAN crystallized in an application of Equation (11). The effects of the pH in the HAN synthesis process on the density of the HAN solution are shown in Figure 2. The concentration of HAN and the density of the sample obtained at pH 5.35 were 37% and 1.27 g/mL, respectively. As the pH increased, the concentration and density increased up to pH 7.06, at which point the concentration and density started to decrease (Figures 1 and 2, respectively). Finally, the concentration and density in the aqueous HAN solution showed the corresponding maximum values at an acidic pH of 7.06; the corresponding values were 60% and 1.39 g/mL.

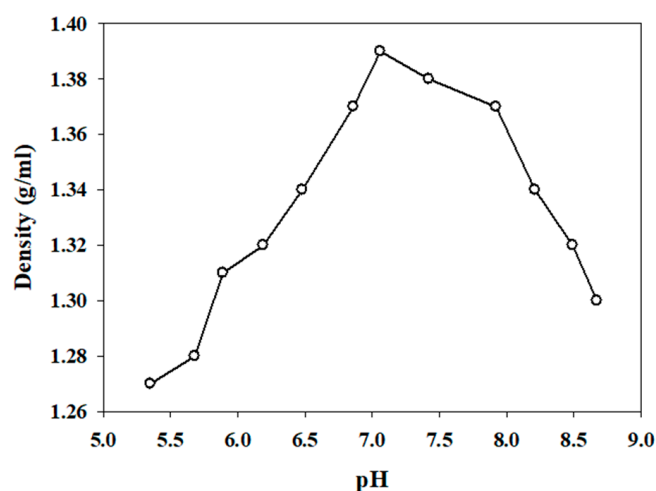


Figure 2. Effects of the pH in the HAN synthesis process on the density of the HAN solution.

On the other hand, if the aqueous solution is concentrated under reduced pressure, it changes to a gel state, and here it was possible to obtain a HAN compound content of 80%.

In this study, due to the deliquescent properties of HAN, the maximum content that could be obtained when the solvent was evaporated to the maximum level could not exceed 80%.

2.2. FT-IR Analysis of Hydroxylammonium Nitrate Solution

In order to examine the synthesis characteristics of ionized HAN compounds in a liquid state, the chemical functional groups of the materials were traced by way of infrared spectroscopy. As shown in the spectrum in Figure 3, the peak spectra of the N-H and O-H functional groups in hydroxylamine, which is the initial reactant, were observed at the points of 3244 cm^{-1} and 1605 cm^{-1} , respectively. The HAN synthesized in this study showed corresponding points of 3324 cm^{-1} and 1608 cm^{-1} , similar to those of the relative peak spectra. By comparing the N-H peak spectra in molecules, it was possible to determine whether ionized HAN existed. It is known theoretically that N-H, O-H, and N-O peaks can be observed at the points of $3500\text{--}3200\text{ cm}^{-1}$, $1600\text{--}1400\text{ cm}^{-1}$, and $1400\text{--}1300\text{ cm}^{-1}$, respectively [33]. Hence, the N-H functional groups could be determined indirectly by analyzing hydroxylamine sulfate ($(\text{NH}_3\text{OH})_2\text{SO}_4$) and ammonium nitrate (NH_4NO_3). In addition, the presence of N-O in the functional groups was determined by observing the peak spectra of potassium nitrate and ammonium nitrate, as shown in Figure 4. Both functional groups were present at levels quite similar to those of the reference materials. Consequently, the materials synthesized in this study were confirmed to be ionized HAN.

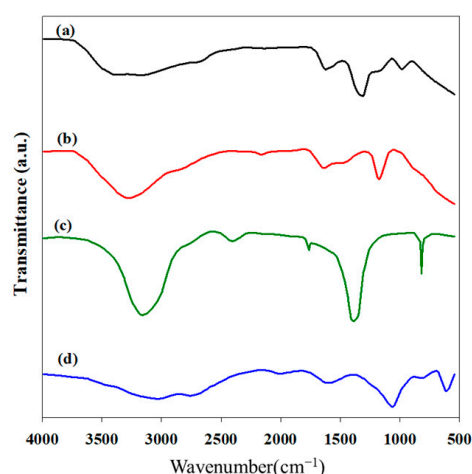


Figure 3. FT-IR spectra of various samples. (a) Synthesized HAN; (b) hydroxylamine; (c) ammonium nitrate; (d) hydroxylamine sulfate.

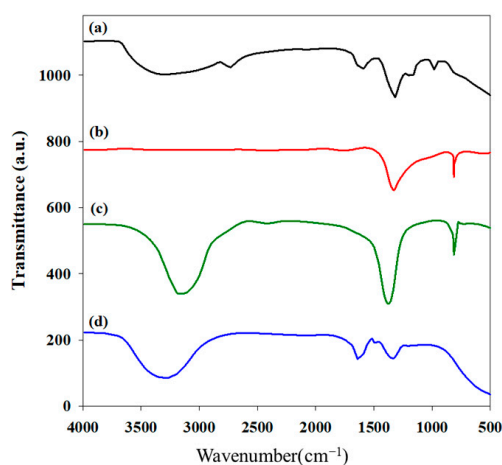


Figure 4. FT-IR spectra of various samples. (a) Synthesized HAN; (b) potassium nitrate; (c) ammonium nitrate; (d) nitric acid.

2.3. Characterization of Metal Oxide/Honeycomb Catalysts

Figure 5 shows scanning electron microscope (SEM) images before and after the pretreatment of the honeycomb support. As shown in Figure 5a, the surface of the honeycomb support was not smooth and contained a large number of impurities prior to the pretreatment. By following the pretreatment procedures, impurities were removed from the surface by means of alkali, acid, and organic solvents, as well as surfactants, in that order. As a result, the surface of the honeycomb support became smooth, as shown in Figure 5b. Figure 6a,b present SEM images of the Pt/honeycomb and Cu/honeycomb catalysts, respectively. The morphology of the catalyst surface on which Pt or Cu was impregnated differed from that in the image taken prior to the coating step (Figure 5b).

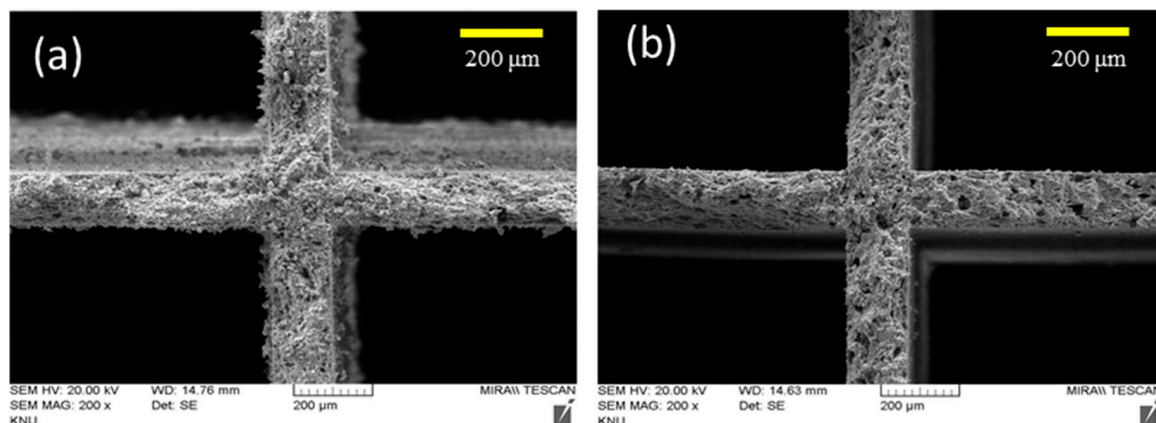


Figure 5. SEM images of honeycomb support (a) before pretreatment and (b) after pretreatment.

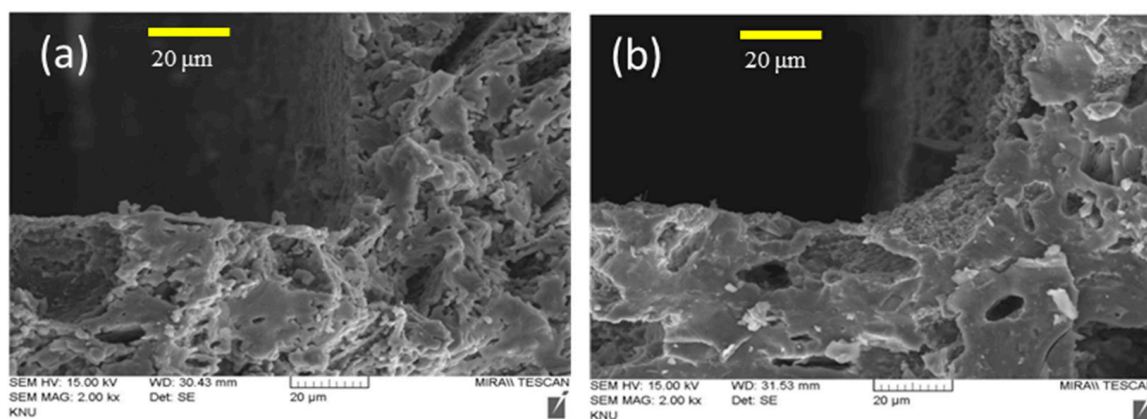


Figure 6. SEM images of (a) Pt/honeycomb and (b) Cu/honeycomb.

The nitrogen adsorption isotherm of the honeycomb (Figure 7) shows that it corresponded to Type III in the International Union of Pure and Applied Chemistry (IUPAC) classification, meaning that the adsorbed molecules were clustered around the most favorable sites on the surface of a nonporous or macroporous solid and that the micropores were mostly undeveloped [34]. Because the Brunauer–Emmett–Teller (BET) surface area of the honeycomb support was as small as $0.1 \text{ m}^2/\text{g}$ or less (Table 1), it was clear that the honeycomb support consisted of nonporous materials. The nitrogen adsorption isotherm of catalysts on which Mn, Co, Cu, Pt, or Ir metallic oxides were impregnated on the honeycomb did not differ greatly from that of the honeycomb support. Thus, it was found that the pore structure of the honeycomb catalysts on which the metallic materials were impregnated did not differ much from that of the honeycomb support. However, the BET surface area of the catalysts on which the Mn, Co, Cu, Pt, or Ir metallic oxides was impregnated on the honeycomb were within the range of $0.62\text{--}1.04 \text{ m}^2/\text{g}$, showing somewhat larger

values than those associated with the surface area of the honeycomb support. This implies that as the metallic oxides were impregnated on the nonporous honeycomb support, some pores were created. The result of the analysis of the nitrogen adsorption isotherm, however, shows that the pore structure of the metal oxide/honeycomb catalysts did not significantly depend on the type of metal loaded.

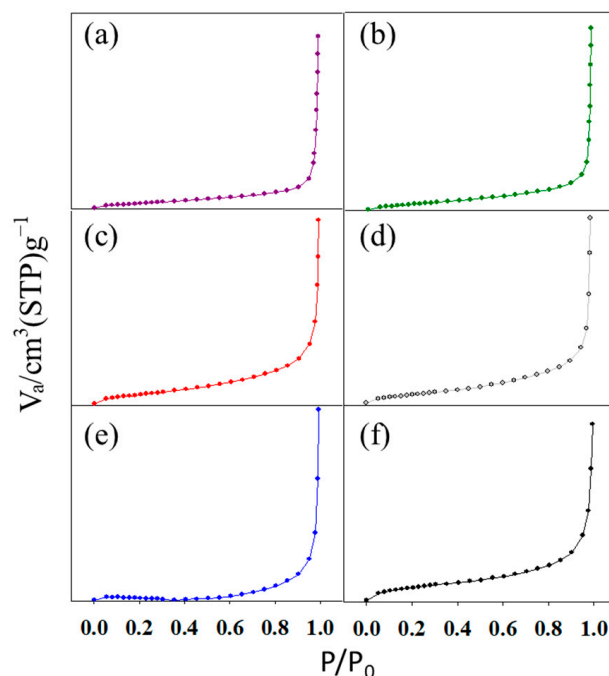


Figure 7. Nitrogen adsorption isotherms of (a) Mn/honeycomb, (b) Co/honeycomb, (c) Pt/honeycomb, (d) Ir/honeycomb, (e) Cu/honeycomb, and (f) honeycomb support.

Table 1. Surface area and pore volume of various catalysts.

Catalyst	BET Surface Area (m ² /g)	Pore Volume (cm ³ /g)
Honeycomb	1.3	0.005
Cu/honeycomb	0.3	0.004
Ir/honeycomb	0.9	0.010
Pt/honeycomb	0.6	0.010
Co/honeycomb	1.0	0.010
Mn/honeycomb	0.8	0.010

Figure 8 shows the results of an X-ray diffraction (XRD) analysis of catalysts on which Mn, Co, Cu, Pt, or Ir metallic oxides were impregnated on the honeycomb. In view of the XRD patterns of the honeycomb support that consisted of MgO-SiO₂-Al₂O₃, it is clear that Mn, Co, Cu, Pt, or Ir metallic oxides were impregnated on the surface of the honeycomb support. The quantities of metals impregnated on the honeycomb support were analyzed by means of X-ray fluorescence (XRF), which showed that amounts in the range of 13.5–17.8 wt% of Mn, Co, Cu, Pt, or Ir elements were impregnated (Table 2).

Table 2. Metal loading over honeycomb support determined by XRF.

Catalyst	Metal Oxide Loading (wt%)
Cu/honeycomb	13.9
Ir/honeycomb	13.5
Pt/honeycomb	14.2
Co/honeycomb	17.8
Mn/honeycomb	15.8

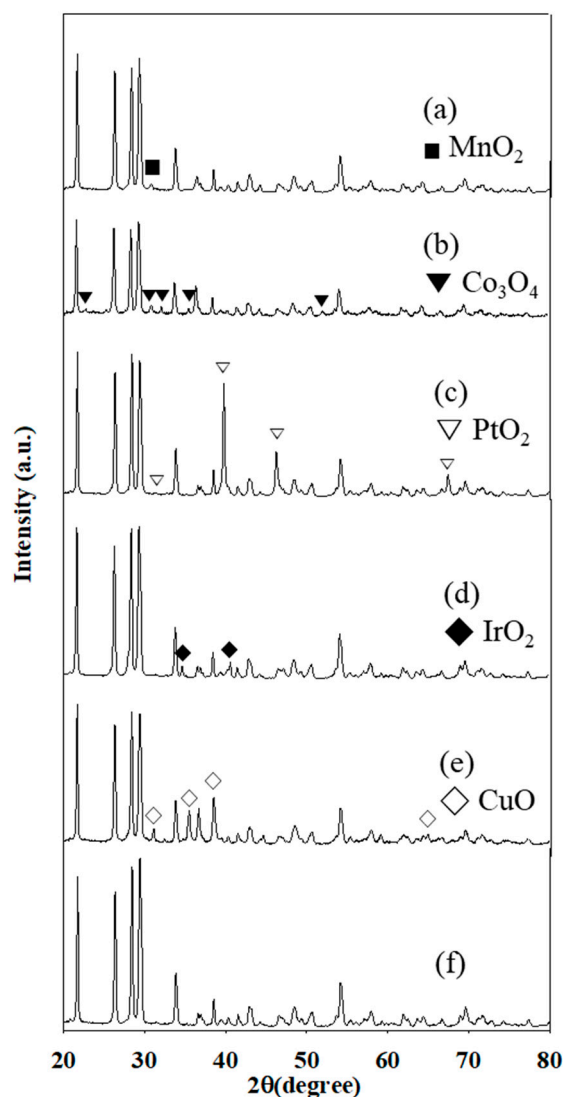


Figure 8. XRD patterns of various catalysts. (a) Mn/honeycomb; (b) Co/honeycomb; (c) Pt/honeycomb; (d) Ir/honeycomb; (e) Cu/honeycomb; (f) honeycomb.

2.4. Thermal and Catalytic Decomposition of the Aqueous HAN Solution

The thermogravimetric analyzer (TGA) thermogram of the HAN solution is shown in Figure 9. The broad endothermic curve up to 120 °C is attributed to the evaporation of water in the aqueous HAN solution. The corresponding weight loss observed in the TG curve is in good agreement with the water content in the HAN solution, as evaluated via density measurements. The aqueous HAN solution (80%) was found to decompose at approximately 124 °C.

Figure 10 shows representative examples of an aqueous HAN solution decomposition by means of the Pt/honeycomb catalysts. This figure indicates the points of inflection that result from intense heat generation at around 52.9 °C. At such points, intense heat caused the catalyst temperature to increase drastically. The point at which the temperature increases is called the decomposition onset temperature (T_{dec}). As gases are also generated as a result of the intense heat at such points, a drastic pressure increase also occurs. The difference between the pressure right before decomposition and the maximum pressure is expressed as ΔP . The temperature of decomposition initiation was low in this case, indicating that the low-temperature decomposition of the catalyst was excellent. The larger the value of ΔP , the better the decomposition performance of the propellant of the catalyst, which is advantageous for the implementation of the specific impulse of the thruster.

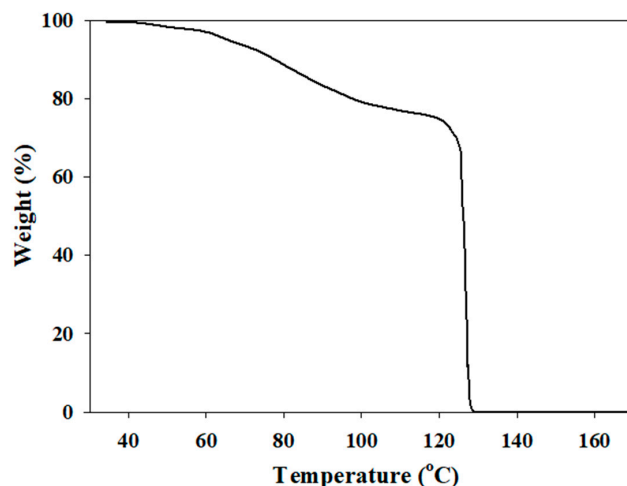


Figure 9. Thermogravimetric analysis of the HAN solution.

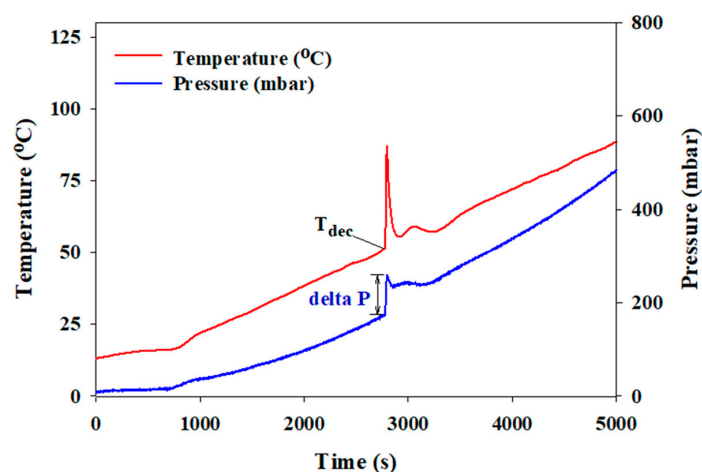


Figure 10. Decomposition temperature and pressure of the HAN solution over the Pt/honeycomb catalyst.

With regard to thermal decomposition without a catalyst during the decomposition reactions of the HAN solution in the batch-type reactor, the decomposition onset temperature was 86.0 °C. In the case of the decomposition of the HAN solution over the cordierite honeycomb without metal deposition, the decomposition onset temperature was 83.0 °C, which means that the cordierite honeycomb without active metal loading played a minor role as a catalyst in lowering the decomposition temperature (Figure 11). The decomposition onset temperatures over the Mn, Pt, Ir, Cu, and Co supported on honeycomb catalysts were measured and found to be 67.8, 52.9, 76.9, 41.0, and 74.7 °C, respectively (Figure 11). To be specific, the Cu/honeycomb catalyst had the effect of lowering the decomposition onset temperature by 45.0 °C compared to during thermal decomposition. The surface area and pore size of the catalysts did not differ significantly. Therefore, the pore structure of the catalyst cannot account for the excellent activity of the Cu/honeycomb. Because the metal-loading amounts did not differ significantly, the greater activity of the Cu/honeycomb catalyst likely arose due to the intrinsic activity of the Cu metal being superior to that of the other metals. It is agreed upon in the literature that Cu oxide has excellent activity in the decomposition reaction of energetic ionic liquid [5,35]. Consequently, it was found that the Cu/honeycomb catalyst, which was prepared by repeating the wash-coating procedure, is an optimal catalyst for the decomposition of an aqueous HAN solution.

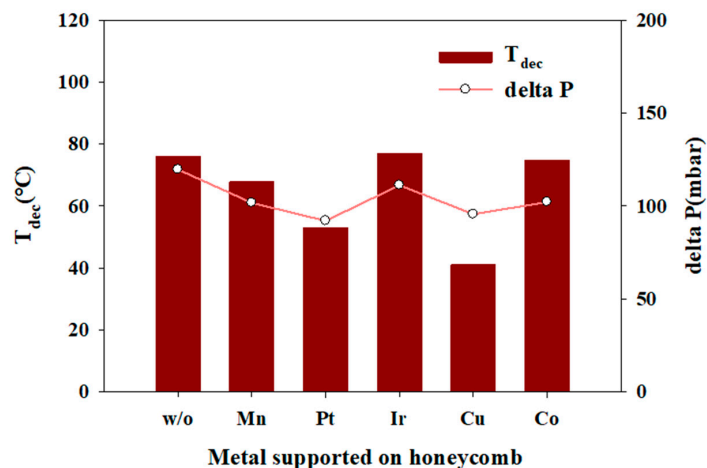


Figure 11. Decomposition onset temperature (T_{dec}) and ΔP in the catalytic decomposition of the HAN solution over various catalysts.

The efficiency of the Cu/Honeycomb catalyst was demonstrated by the decreased decomposition onset temperature of 41 °C instead of 86 °C for the thermal process of the HAN solution. The catalytic effect of the Cu/honeycomb catalyst was clearly evidenced by the decreased decomposition onset temperature in comparison with thermal decomposition. Low decomposition onset temperatures circumvent the preheating of the catalyst bed of the thruster, thus reducing the energy supply [9].

The product gases collected from the catalytic decomposition of the HAN solution over the catalysts were analyzed using an infrared spectrometer. As shown in Figure 12, Fourier-transform infrared spectroscopy (FT-IR) absorbance bands associated with HNO_2 , N_2O and NO_2 were observed [36–38]. These species are intermediates included in the thermal decomposition pathways (Equations (2)–(9)) of the aqueous HAN solution, as suggested in a previous report [26]. The FT-IR absorbance bands obtained from the catalytic decomposition reaction were similar to those obtained from the thermal decomposition process and were not significantly affected by the type of catalyst used. This means that the effect of the catalyst on the decomposition mechanism of the aqueous HAN solution was negligible.

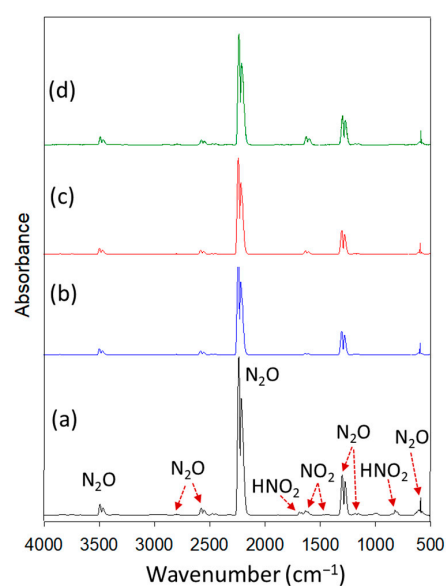


Figure 12. FT-IR spectra of gas generated during the decomposition of the HAN solution. FT-IR spectra of gas generated during the decomposition of the HAN solution. (a) Thermal; (b) Cu/honeycomb; (c) Pt/honeycomb; (d) Ir/honeycomb.

2.5. Catalyst Reusability Test

In order to verify the reusability of the Cu/honeycomb catalyst, the decomposition experiments on the aqueous HAN solution were repeated 19 times and the values of T_{dec} and ΔP versus the time were obtained (Figure 13). During the 19 repeated decomposition trials of the aqueous HAN solution, T_{dec} and ΔP were maintained at a constant level over the Cu/honeycomb catalyst.

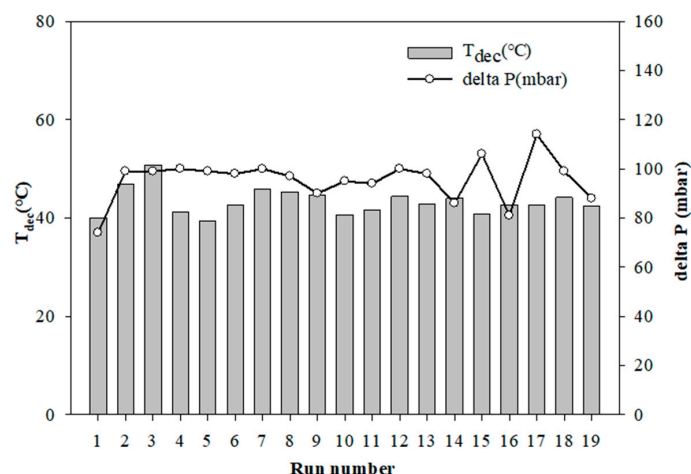


Figure 13. Decomposition onset temperature (T_{dec}) and ΔP in the repeated decomposition of the HAN solution over the Cu/honeycomb catalyst.

Once decomposition of a liquid propellant starts in an artificial satellite thruster, ignition is initiated and the catalyst bed temperature increases intermittently to as high as 1200 °C. In order to evaluate the heat resistance of the catalysts, an experiment was conducted in which a thermal shock was applied to the catalysts. After a thermal treatment for the Cu/honeycomb catalysts in a furnace at 1200 °C lasting approximately ten minutes, they were cooled to room temperature and then put into a reactor for the aqueous HAN solution decomposition experiment. To the best of our knowledge, this heat resistance study is the first to evaluate the heat resistance as well as the decomposition activity of a honeycomb-type catalyst during the decomposition of an aqueous HAN solution. After the cycle of thermal shock application and aqueous HAN solution decomposition was repeated five times, there was an insignificant difference in both T_{dec} and ΔP (Figure 14). Hence, at 1200 °C, the deactivation of Cu/honeycomb catalysts is negligible. Accordingly, it was confirmed that the Cu/honeycomb catalyst could be recovered and reused as a catalyst for the decomposition of a HAN-based liquid monopropellant.

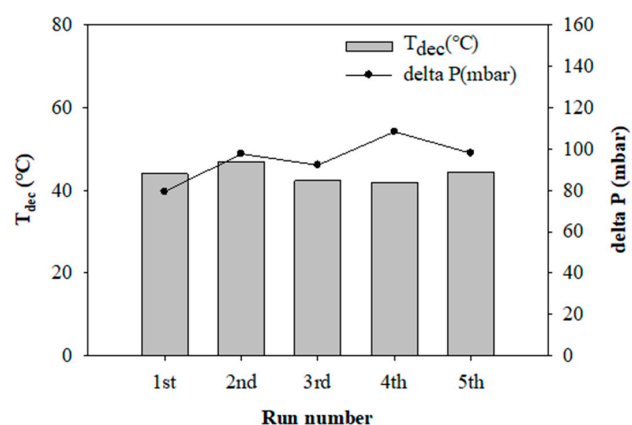


Figure 14. Decomposition onset temperature (T_{dec}) and ΔP in repeated decomposition of the HAN solution over the Cu/honeycomb catalyst (thermal shock was applied to the catalyst between each run).

3. Experimental Details

3.1. Synthesis of Hydroxylammonium Nitrate

As raw materials for HAN synthesis, this study utilized nitric acid (assay—60%, Daejung Chemical & Metals Co., Ltd.) and hydroxylamine (assay—50%, Sigma-Aldrich, Louis, MO, USA). A total of 95% high-density nitric acid was extracted through a dehydration reaction of 60% nitric acid and high-density sulfuric acid (98%, Sigma-Aldrich, Louis, MO, USA). If the hydroxylamine (assay—50%, NH₂OH, Sigma-Aldrich, Louis, MO, USA) solution contained a small quantity of metallic elements, the reaction shown in Equation (12) could have occurred in the titration process [39].



Since such metallic ions could cause hydroxylamine decomposition, the manufacturing of HAN by means of high-purity hydroxylamine could have been hindered as a result. Accordingly, a small quantity of metallic elements and other impurities were filtered by means of a membrane filter (PTFE, Sigma-Aldrich, Louis, MO, USA) in this study. For HAN synthesis, high-purity hydroxylamine solution was used with 95% density nitric acid and impurities were removed. Nitric acid was added drop by drop to a 3-neck flask with hydroxylamine in it (1 mL/min), and the temperature in the synthesis reactor was consistently less than 50 °C.

3.2. Analysis of Hydroxylammonium Nitrate

Functional groups of N-H and N-O inside the synthesized HAN compound aqueous solution were detected by means of FT-IR (Spectrum One System, Perkin-Elmer, Waltham, MA, USA). In addition, the ionized HAN was analyzed quantitatively in comparison with ammonium nitrate, hydroxylamine, and hydroxylamine sulfate, which have structures similar to that of HAN. The pyrolysis temperature of the synthesized HAN was measured by means of thermogravimetric analysis (TGA N-1500, Scinco, Seoul, Korea). The specific gravity of the aqueous HAN solution was measured, and the relative content of HAN in the aqueous phase was calculated with Equation (11) [32].

3.3. Preparation of the Catalysts

The honeycomb supports used here were purchased from Ceracomp Co. Ltd (Cheonan, Korea). The chosen material was cordierite (MgO-SiO₂-Al₂O₃) and the monolith displayed 18 × 18 square channels with internal side lengths of one inch. As shown in Figure 15, impurities on the surface were removed by means of alkali, acid, and organic solvents as well as surfactants in order to facilitate the coating of metallic oxide on the honeycomb surface [40]. The honeycomb (1 cm in length and 1 cm in diameter) was immersed in a 1 M sodium hydroxide solution (NaOH, Sigma-Aldrich, Louis, MO, USA, 98%) and an ultrasonic wave treatment was applied for 15 min. The honeycomb was then immersed in a 0.5M hydrochloric acid solution (HCl, Sigma-Aldrich, Louis, MO, USA, 35~37%), after which another ultrasonic wave (Jeio Tech, Daejeon, Korea) treatment was conducted for 15 min. This honeycomb was calcined under an air atmosphere at 900 °C for 12 h. The calcined honeycomb was immersed in toluene for sonication, dried in an oven at 100 °C, and then washed with distilled water. Moisture in the honeycomb was dried in the oven (Jeio Tech, Daejeon, Korea) at 100 °C and then dipped in hexadecyltrimethylammonium bromide (CTABr, Sigma-Aldrich, Louis, MO, USA, >98%) for five hours.

The impregnation of metals, in this case, Mn, Co, Cu, Pt, and Ir, was performed by means of the wet impregnation coating method on the honeycomb support. The metallic precursors that were used were manganese nitrate tetrahydrate (Sigma-Aldrich, Louis, MO, USA, 97%), cobalt nitrate hexahydrate (Sigma-Aldrich, Louis, MO, USA, 97%), copper nitrate trihydrate (Sigma-Aldrich, Louis, MO, USA, 78.5%), palladium chloride (Sigma-Aldrich, Louis, MO, USA, 99%), platinum chloride (Kojima Chemicals, Sayama, Japan, 99%), and hydrogen hexachloroiridate hydrate (H₂Cl₆Ir·xH₂O, Sigma-Aldrich, Louis, MO,

USA, 99%). The pretreated honeycomb support was dipped in the metallic precursor solution and the solvents were evaporated twice for four hours in each case at 70 °C, with the pressure reduced by means of a rotary evaporator. Drying for four hours at 110 °C was followed by a thermal treatment at 1200 °C to finalize the honeycomb catalyst coated with metallic oxide (Figure 16).

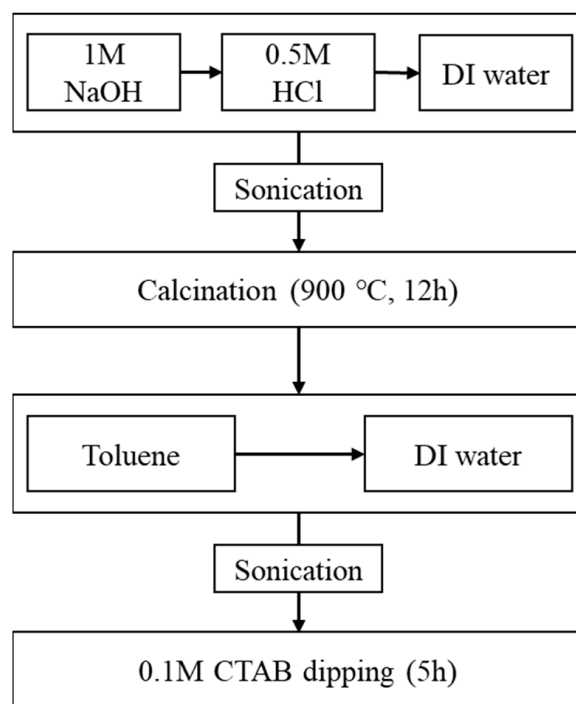


Figure 15. Pretreatment procedure for the honeycomb support.

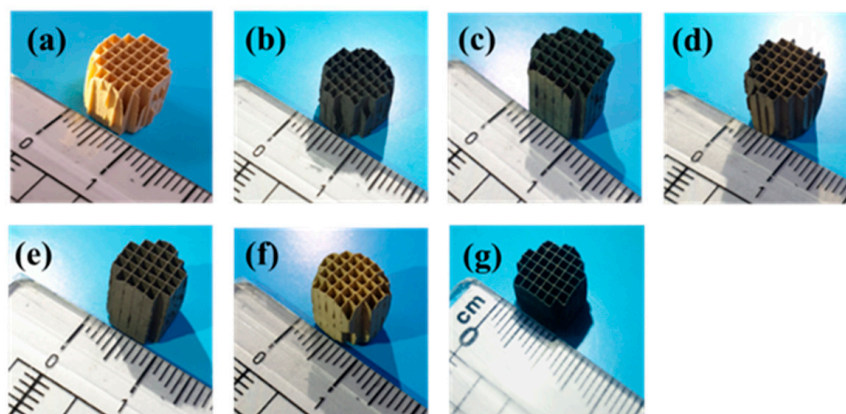


Figure 16. Metal oxide catalysts supported on honeycomb. (a) Cordierite honeycomb; (b) Cu; (c) Co; (d) Mn; (e) Pt; (f) Ir; (g) Pd.

Once a liquid propellant starts to decompose in an artificial satellite thruster, ignition is initiated and the catalyst bed temperature increases intermittently to as high as 1200 °C. Accordingly, the metal oxide/honeycomb used in this study was calcined at 1200 °C during the final step of the catalyst preparation procedure. If calcination was performed at 1200 °C after washcoating Al₂O₃ onto the honeycomb surface, alumina would have been very easily transformed into a non-porous α-Al₂O₃ phase. Maleix et al. showed that non-porous α-Al₂O₃ is inferior to cordierite as a support for a monolith catalyst with regard to the decomposition of an ADN-based monopropellant [5]. Referring to the results of

Maleix et al., metal oxide was directly impregnated over the cordierite honeycomb surface without using an Al_2O_3 washcoat in this study.

3.4. Characterization of the Catalysts

The nitrogen adsorption isotherm was measured at -196°C by means of a BELSORP-mini II device by BEL JAPAN (Osaka, Japan). After treatment of the catalyst specimen in a vacuum at 200°C for six hours, the quantity of adsorption was measured while nitrogen flowed into the adsorption gas at the temperature of liquid nitrogen. The specific surface area was calculated by applying the BET equation, and the entire volume and the average diameter of the pores were calculated by applying the Barrett–Joyner–Halenda (BJH) equation.

The crystallinity of the catalyst was examined by means of XRD. The XRD used here was the MiniFlex600 model by Rigaku (Tokyo, Japan). The measurement angle was between 3° and 90° , and the angular velocity was $5^\circ/\text{min}$. XRD pattern data were collected by means of a Rigaku D/teX ultra-diffractometer (Tokyo, Japan) with a Cu tube and a graphite monochromator mounted on it.

In order to determine the composition of the catalyst, the XRF was measured. A Rigaku/ZSX Primus II device (Tokyo, Japan) was utilized for this, and the district target element was Rh. An image of the catalyst particles was analyzed by means of SEM. A TESCAN/MIRA3-LM (Brno, Czech Republic) high-resolution scanning electron microscope (HR FE-SEM) was utilized. The acceleration voltage was 20 kV.

3.5. Catalytic Decomposition of the HAN Solution

The HAN solution used in this study was composed of 80 wt% HAN and 20 wt% water. The decomposition reaction of the HAN solution was carried out in a custom-made batch-type reactor (Hanwoul Engineering, Gunpo, Korea) (Figure 17) based on earlier work [10,35,41]. The decomposition reaction of the liquid monopropellants proceeded as follows: First, 0.3 g of catalyst was loaded into a sample holder inside the reactor, after which 100 μL of the HAN solution were added using a micropipette (Sigma-Aldrich, Louis, MO, USA). The temperature of the sample holder inside the reactor was raised to 200°C at a rate of $1^\circ\text{C}/\text{min}$. At that time, the pressure and the temperature of the gas phase were recorded ten times per second.

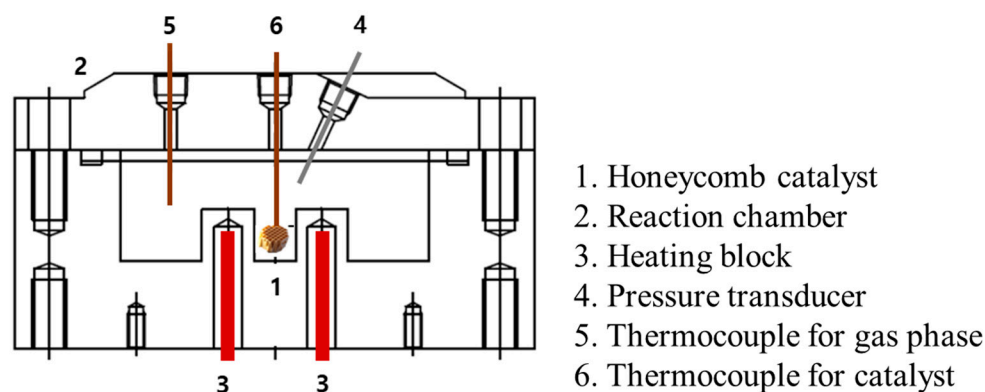


Figure 17. Schematic diagram of the reactor for the decomposition of the propellant.

The gases generated upon decomposition were captured by means of a Tedlar bag (Sigma-Aldrich, Louis, MO, USA) injected with heatable gas cells from PerkinElmer in a vacuum and analyzed by means of FT-IR (Spectrum Two FT-IR by PerkinElmer, Waltham, MA, USA).

4. Conclusions

Hydroxylammonium nitrate was prepared via a neutralization reaction of hydroxylamine and nitric acid. FT-IR was used to analyze the chemical composition, chemical

structure, and functional groups of the HAN. The aqueous HAN solution obtained at pH 7.06 showed the highest concentration of HAN at 60% and a density of 1.39 g/mL. The concentration of HAN solution that could be obtained when the solvent was evaporated to the maximum level could not exceed 80%.

A total of 13.5–17.8 wt% of Mn, Co, Cu, Pt, or Ir metals were impregnated onto a honeycomb support composed of cordierite ($\text{MgO-SiO}_2\text{-Al}_2\text{O}_3$). The pore structure of the metal oxide/honeycomb catalysts did not significantly depend on the type of metal loaded. The Cu/honeycomb catalyst showed the strongest effect of lowering the decomposition onset temperature during the decomposition of the HAN solution, which was likely due to the intrinsic activity of the Cu metal being superior to that of the other metals. It was confirmed that the effect of the catalyst on the decomposition mechanism of the aqueous HAN solution was negligible. Through a repetitive cycle of the application of a thermal shock and decomposition of an aqueous HAN solution, it was confirmed that the Cu/honeycomb catalyst could be recovered and reused as a catalyst for the decomposition of an aqueous HAN solution.

Author Contributions: Conceptualization, Y.J. and J.-K.J.; Methodology, Y.J.; Formal analysis, D.Y., M.K. and S.K.; Investigation, D.Y., S.K.O., W.K. and Y.K.; Data curation, D.Y. and M.K.; Writing—original draft, S.H. and J.-K.J.; Project administration, J.-K.J.; Funding acquisition, J.-K.J. All authors have read and agreed to the published version of the manuscript.

Funding: This research was funded by a research grant from the Kongju National University in 2022.

Data Availability Statement: Data are contained within the article.

Conflicts of Interest: The authors declare no conflict of interest.

References

1. McKechnie, T.; Shchetkovskiy, A. Development of Metallic Foams monolithic Catalysts for Green Monopropellants Propulsion. In Proceedings of the Space Propulsion Conference, Rome, Italy, 2–6 May 2016; p. 232.
2. Amrousse, R.; Katsumi, T.; Azuma, N.; Hori, K. Hydroxylammonium nitrate (HAN)-based green propellant as alternative energy resource for potential hydrazine substitution: From lab scale to pilot plant scale-up. *Combust. Flame* **2017**, *176*, 334–348. [[CrossRef](#)]
3. Courtheoux, L.; Gautron, E.; Rossignol, S.; Kappenstein, C. Transformation of platinum supported on silicon-doped alumina during the catalytic decomposition of energetic ionic liquid. *J. Catal.* **2005**, *232*, 10–18. [[CrossRef](#)]
4. Oommen, C.; Rajaraman, S.; Chandru, R.A.; Rafeev, R. Catalytic Decomposition of Hydroxylammonium Nitrate Monopropellant. In Proceedings of the International Conference on Chemistry and Chemical Process, Bangkok, Thailand, 7–9 May 2011; p. 10.
5. Maleix, C.; Chabernaud, P.; Brahmi, R.; Beauchet, R.; Batonneau, Y.; Kappenstein, C.; Schwentenwein, M.; Koopmans, R.J.; Schuh, S.; Scharlemann, C. Development of catalytic materials for decomposition of ADN-based monopropellants. *Acta Astronaut.* **2019**, *158*, 407–415. [[CrossRef](#)]
6. Neto, T.G.S.; Ferreira, J.G.; Cobo, A.J.G.; Cruz, G.M. Ir-Ru/ Al_2O_3 catalysts used in satellite propulsion. *Brazhlan J. Chem. Eng.* **2003**, *20*, 273–282. [[CrossRef](#)]
7. Masse, R.; Spores, A.R.; Kimbrel, S.; Allen, M.; Lorimor, E.; Myers, P. GPIM AF-M315E Propulsion System. In Proceedings of the 50th AIAA/ASME/SAE/ASEE Joint Propulsion Conference, Cleveland, OH, USA, 28–30 July 2014; pp. 2015–3753.
8. Jang, I.J.; Jang, Y.B.; Shin, H.S.; Shin, N.R.; Kim, S.K.; Yu, M.J.; Cho, S.J. Preparation and characterization of lanthanum hexaaluminate granule for catalytic application in aerospace technology. In Proceedings of the 18th International Conference on Composite Materials, Jeju, Korea, 21–26 August 2011.
9. Amrousse, R.; Hori, K.; Fetimi, W.; Farhat, K. HAN and ADN as liquid ionic monopropellants: Thermal and catalytic decomposition processes. *Appl. Catal. B Environ.* **2012**, *127*, 426–428. [[CrossRef](#)]
10. Hong, S.; Heo, S.; Kim, W.; Jo, Y.M.; Park, Y.K.; Jeon, J.K. Catalytic decomposition of an energetic ionic liquid solution over hexaaluminate catalysts. *Catalysts* **2019**, *9*, 80. [[CrossRef](#)]
11. Chai, W.S.; Cheah, K.H.; Koh, K.S.; Chin, J.; Chik, T.F.W.K. Parametric studies of electrolytic decomposition of hydroxylammonium nitrate (HAN) energetic ionic liquid in microreactor using image processing technique. *Chem. Eng. J.* **2016**, *296*, 19–27. [[CrossRef](#)]
12. Shobaky, G.A.E.; Turky, A.E.M.M. Catalytic decomposition of H_2O_2 on Co_3O_4 doped with MgO and V_2O_5 . *Colloids Surfaces* **2000**, *170*, 161–172. [[CrossRef](#)]
13. Xiaoguang, R.; Minghui, L.; Ai Qin, W.; Lin, L.; Xiaodong, W.; Zhang, T. Catalytic decomposition of hydroxyl ammonium nitrate at room temperature. *Chin. J. Catal.* **2007**, *28*, 1–2.
14. Kang, S.J. Evaluation of Catalytic Decomposition Performance for 1 n Class Ionic Liquid Monopropellant Thruster. Master's Thesis, Korea Advanced Institute of Science and Technology, Daejeon, Korea, 2012.

15. Sam, I.I.; Gayathri, S.; Santhosh, G.; Cyriac, J.; Reshmi, S. Exploring the possibilities of energetic ionic liquids as non-toxic hypergolic bipropellants in liquid rocket engines. *J. Mol. Liq.* **2022**, *350*, 118–217.
16. Kang, L.; Liu, J.; Yao, Y.; Wu, X.; Zhang, J.; Zhu, C.G.; Xu, F.; Xu, S. Enhancing risk/safety management of HAN-based liquid propellant as a green space propulsion fuel: A study of its hazardous characteristics. *Process Saf. Environ. Prot.* **2023**, *177*, 921–931. [[CrossRef](#)]
17. Nosseir, A.E.S.; Cervone, A.; Pasini, A. Review of state-of-the-art green monopropellants: For propulsion systems analysts and designers. *Aerospace* **2021**, *8*, 20. [[CrossRef](#)]
18. Masse, R.K.; Allen, M.; Spores, R.A.; Driscoll, E. AF-M315E Propulsion System Advances & Improvements. In Proceedings of the 52nd AIAA/SAE/ASEE Joint Propulsion Conference, Salt Lake City, UT, USA, 25–27 July 2016.
19. Neff, G.A. The Decomposition of Hydroxylammonium Nitrate under Vacuum Conditions. Master's Thesis, University of West Michigan, Kalamazoo, MI, USA, 2016.
20. Liggett, T. Process for Producing Concentrated Solutions of Hydroxylammonium Nitrate and Hydroxylammonium Perchlorate. U.S. Patent 4066736A, 3 January 1978.
21. Wagaman, K.L. Synthesis of Hydroxylamine Salts. U.S. Patent 4956168A, 11 September 1990.
22. Liggett, T. Hydroxylammonium Nitrate Process. U.S. Patent 5182092A, 26 January 1993.
23. Coates, J. Interpretation of infrared spectra, a practical approach. In *Encyclopedia of Analytical Chemistry*; John Wiley & Sons Ltd: Hoboken, NJ, USA, 2000; pp. 10815–10837.
24. Cawfield, D.W. Process for the Production of High Purity Hydroxylammonium Nitrate. U.S. Patents 5213784A, 25 May 1993.
25. Hong, S.; Heo, S.; Jo, Y.M.; Kim, T.; Jeon, J.K. A Study on Nanoporous Catalysts for Decomposition of AND-Based Liquid Monopropellant. *Korean Soc. Propuls. Eng.* **2016**, *47*, 1319–1322.
26. Lee, H.S.; Litzinger, T.A. Chemical kinetic study of HAN decomposition. *Combust. Flame* **2003**, *135*, 151–169. [[CrossRef](#)]
27. Giani, L.; Cristiani, C.; Groppi, G.; Tronconi, E. Washcoating method for Pd/ γ -Al₂O₃ deposition on metallic foams. *Appl. Catal. B Environ.* **2006**, *62*, 121–131. [[CrossRef](#)]
28. Jiang, P.; Lu, G.; Guo, Y.; Zhang, Y.; Wang, X. Preparation and properties of a γ -Al₂O₃ washcoat deposited on a ceramic honeycomb. *Surf. Coat. Technol.* **2005**, *190*, 314–320. [[CrossRef](#)]
29. Kotani, W.; Hamaguchi, K.; Kasai, Y. Ceramic Honeycomb Structure with Grooves and Outer Coating, Process of Producing the Same, and Coating Material Used in the Honeycomb Structure. U.S. Patent 5629067A, 13 May 1997.
30. Shamshuddin, S.Z.M.; Sundar, M.S.; Thimmaraju, N.; Vatsalya, V.G.; Senthilkumar, M. Synthesis, characterization and catalytic activity studies on cordierite honeycomb coated with ZrO₂ based solid super acids. *Comptes Rendus Chim.* **2012**, *15*, 799–807. [[CrossRef](#)]
31. Agnihotri, R.; Oommen, C. Cerium oxide based active catalyst for hydroxylammonium nitrate (HAN) fueled monopropellant thrusters. *RSC Adv.* **2018**, *8*, 22293–22302. [[CrossRef](#)]
32. Chai, W.S. Characterization & Analysis on Electrolytic Decomposition of Hydroxylammonium Nitrate (HAN) Ternary Mixtures in Microreactors. Ph.D. Thesis, University of Nottingham, Nottingham, UK, 2017.
33. Kuo, B.H. A Study on the Electrolytic Decomposition of HAN-Based Propellants for Microthruster Applications. Master's Thesis, Pennsylvania State University, University Park, PA, USA, 2010.
34. Thommes, M.; Kaneko, K.; Neimark, A.V.; Olivier, J.P.; Reinoso, F.R.; Rouquerol, J.; Sing, K.S.W. Physisorption of gases, with special reference to the evaluation of surface area and pore size distribution (IUPAC Technical Report). *Pure Appl. Chem.* **2015**, *87*, 1051–1069. [[CrossRef](#)]
35. Heo, S.; Kim, M.; Lee, J.; Park, Y.C.; Jeon, J.K. Decomposition of ammonium dinitramide-based liquid propellant over Cu/hexaaluminate pellet catalysts. *Korean J. Chem. Eng.* **2019**, *36*, 660–668. [[CrossRef](#)]
36. Pipa, A.V.; Röpkke, J. Analysis of the Mid-Infrared Spectrum of the Exhaust Gas From an Atmospheric Pressure Plasma Jet (APPJ) Working With an Argon–Air Mixture. *IEEE Trans. Plasma Sci.* **2009**, *37*, 1000–1003. [[CrossRef](#)]
37. Dorhout, J.M.; Anderson, A.S.; Batista, E.; Carlson, R.K.; Currier, R.P.; Martinez, R.K.; Clegg, S.M.; Wilkerson, M.P.; Nowak-Lovato, K. NO_x speciation from copper dissolution in nitric acid/water solutions using FTIR spectroscopy. *J. Mol. Spec.* **2020**, *372*, 111334. [[CrossRef](#)]
38. National Institute of Standards and Technology (NIST) Chemistry WebBook, SRD 69. Available online: <https://webbook.nist.gov/cgi/cbook.cgi?ID=C10024972&Type=IR-SPEC&Index=1> (accessed on 25 January 2024).
39. Bengtsson, G.; Fronæus, S.; Kloo, L.B. The kinetics and mechanism of oxidation of hydroxylamine by iron (III). *J. Chem. Soc., Dalton Trans.* **2002**, *12*, 2548–2552. [[CrossRef](#)]
40. Yun, Y.; Kim, E.; Lee, B.; Ko, T.; Oh, J. The microstructure of Magnetite Coated on Honeycomb and Characteristics of CO₂ Decomposition. *J. Korean Ceram. Soc.* **2004**, *41*, 410–416.
41. Yoo, D.; Woo, J.; Oh, S.; Jeon, J.K. Performance of Pt and Ir Supported on Mesoporous Materials for Decomposition of Hydroxylammonium Nitrate Solution. *J. Nanosci. Nanotechnol.* **2020**, *20*, 4461–4465. [[CrossRef](#)]

Disclaimer/Publisher's Note: The statements, opinions and data contained in all publications are solely those of the individual author(s) and contributor(s) and not of MDPI and/or the editor(s). MDPI and/or the editor(s) disclaim responsibility for any injury to people or property resulting from any ideas, methods, instructions or products referred to in the content.